SINTEF
PROCEEDINGS
1

Selected papers from 10th International Conference on Computational Fluid Dynamics in the Oil & Gas, Metallurgical and Process Industries

Progress in Applied CFD

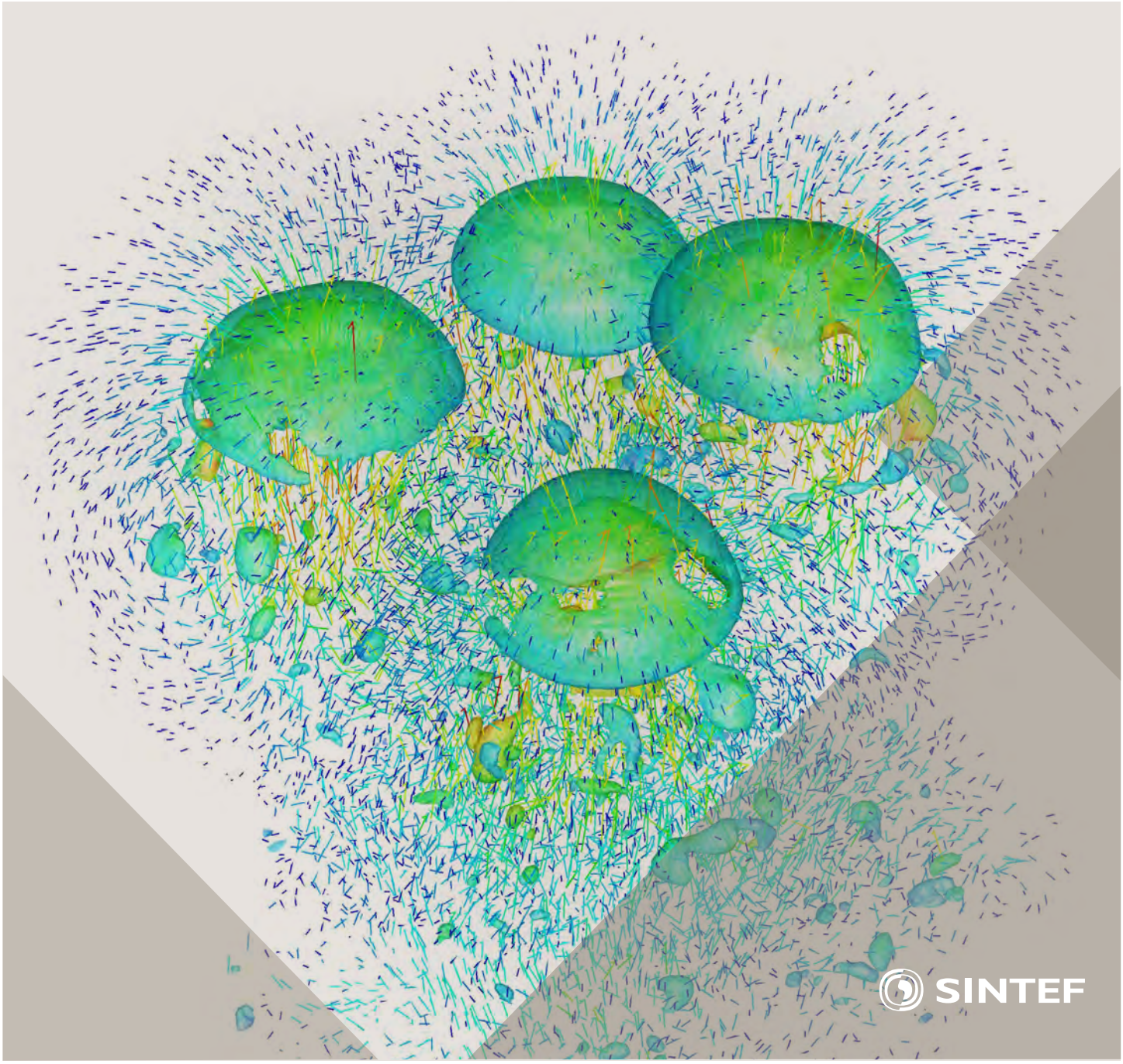

SINTEF Proceedings

Editors:
Jan Erik Olsen and Stein Tore Johansen

Progress in Applied CFD

Selected papers from 10th International Conference on Computational Fluid Dynamics in the Oil & Gas, Metallurgical and Process Industries

SINTEF Academic Press

SINTEF Proceedings no 1
Editors: Jan Erik Olsen and Stein Tore Johansen
Progress in Applied CFD
Selected papers from 10th International Conference on Computational Fluid Dynamics in the Oil & Gas, Metallurgical and Process Industries

Key words:
CFD, Flow, Modelling

Cover, illustration: Rising bubbles by Schalk Cloete

ISSN 2387-4287 (printed)
ISSN 2387-4295 (online)
ISBN 978-82-536-1432-8 (printed)
ISBN 978-82-536-1433-5 (pdf)

60 copies printed by AIT AS e-dit
Content: 100 g munken polar
Cover: 240 g trucard

SINTEF Academic Press
Address: Forskningsveien 3 B
PO Box 124 Blindern
N-0314 OSLO
Tel: +47 22 96 55 55
Fax: +47 22 96 55 08

www.sintef.no/byggforsk
www.sintefbok.no

SINTEF Proceedings
SINTEF Proceedings is a serial publication for peer-reviewed conference proceedings on a variety of scientific topics.
The processes of peer-reviewing of papers published in SINTEF Proceedings are administered by the conference organizers and proceedings editors. Detailed procedures will vary according to custom and practice in each scientific community.

PREFACE

This book contains selected papers from the 10th International Conference on Computational Fluid Dynamics in the Oil & Gas, Metallurgical and Process Industries. The conference was hosted by SINTEF in Trondheim in June 2014 and is also known as CFD2014 for short. The conference series was initiated by CSIRO and Phil Schwarz in 1997. So far the conference has been alternating between CSIRO in Melbourne and SINTEF in Trondheim. The conferences focus on the application of CFD in the oil and gas industries, metal production, mineral processing, power generation, chemicals and other process industries. The papers in the conference proceedings and this book demonstrate the current progress in applied CFD.

The conference papers undergo a review process involving two experts. Only papers accepted by the reviewers are presented in the conference proceedings. More than 100 papers were presented at the conference. Of these papers, 27 were chosen for this book and reviewed once more before being approved. These are well received papers fitting the scope of the book which has a slightly more focused scope than the conference. As many other good papers were presented at the conference, the interested reader is also encouraged to study the proceedings of the conference.

The organizing committee would like to thank everyone who has helped with paper review, those who promoted the conference and all authors who have submitted scientific contributions. We are also grateful for the support from the conference sponsors: FACE (the multiphase flow assurance centre), Total, ANSYS, CD-Adapco, Ascomp, Statoil and Elkem.

Stein Tore Johansen & Jan Erik Olsen

Organizing committee:

Conference chairman: Prof. Stein Tore Johansen
Conference coordinator: Dr. Jan Erik Olsen
Dr. Kristian Etienne Einarsrud
Dr. Shahriar Amini
Dr. Ernst Meese
Dr. Paal Skjetne
Dr. Martin Larsson
Dr. Peter Witt, CSIRO

Scientific committee:

J.A.M.Kuipers, TU Eindhoven
Olivier Simonin, IMFT/INP Toulouse
Akio Tomiyama, Kobe University
Sanjoy Banerjee, City College of New York
Phil Schwarz, CSIRO
Harald Laux, Osram
Josip Zoric, SINTEF
Jos Derksen, University of Aberdeen
Dieter Bothe, TU Darmstadt
Dmitry Eskin, Schlumberger
Djamel Lakehal, ASCOMP
Pär Jonsson, KTH
Ruben Shulkes, Statoil
Chris Thompson, Cranfield University
Jinghai Li, Chinese Academy of Science
Stefan Pirker, Johannes Kepler Univ.
Bernhard Müller, NTNU
Stein Tore Johansen, SINTEF
Markus Braun, ANSYS

CONTENTS

COMPARING EULER-EULER AND EULER-LAGRANGE BASED MODELLING APPROACHES FOR GAS-PARTICLE FLOWS

Markus BRAUN[1], Markus LAMBERT[1], Shailesh OZARKAR[2]*, Jay SANYAL[2]

[1] ANSYS Germany GmbH, Birkenweg 14a, D-64295 Darmstadt, Germany

[2] ANSYS Inc., 275 Technology Drive, Canonsburg, PA, 15317, US

* E-mail: shailesh.ozarkar@ansys.com

ABSTRACT

Comparative assessment of Euler-Euler and Euler-Lagrange modelling approaches for gas-particle flows is performed by comparing their predictions against experimental data of two fluidization challenge problems put forth by National Energy Technology Laboratory (NETL), Morgantown, WV, USA. The first fluidization challenge problem is based on a laboratory scale fluidized bed while the second fluidization challenge problem is based on a pilot scale circulating fluidized bed. It is found that both computational models predict comparable results and those results are in qualitative agreement with the experimental data.

Keywords: Euler-Euler, Euler-Lagrange, Gas-Particle flows, Fluidized bed.

NOMENCLATURE

Greek Symbols

ϕ	Volume fraction of particles.
δ	Normal overlap, [m].
γ	Damping coefficient, [kg/s].
μ	Coefficient of friction.
η	Coefficient of restitution.

Latin Symbols

$\vec{u}_p$	Velocity of a particle p, [m/s].
$\vec{F}$	Various forces acting on a particle, [N].
$\vec{F}_1$	Normal contact force acting on particle 1, [N].
Re_m	Mean flow Reynolds number.
d_p	Diameter of a particle, [m].
m_i	Mass of a particle i, [kg].
m_{12}	Reduced mass, [kg].
K	Normal spring constant, [N/m].
$\vec{e}_{12}$	Unit vector defined from particle 1 to particle 2.
$\vec{v}_{12}$	Relative velocity, [m/s].
t_{coll}	Time scale of collision, [s].

INTRODUCTION

Simulations of gas-particle flows in commercial scale devices such as fluidized beds are of interest to many industries including chemical processing, oil and gas, and energy. For these simulations, traditional Euler-Euler models based on kinetic theory of granular flow (KTGF) along with classical or refined form of gas-particle drag law are routinely used, (Gidaspow et al, 1992; Igci and Sundaresan, 2011; Li and Kwauk, 1994; Milioli et al, 2013; Parmentier et al, 2012; Wen and Yu, 1966). With recent advances in computing power and computational algorithms, there is a growing interest in using Euler-Lagrange models since these models are well suited for accounting for particle size distributions in comparison to Euler-Euler KTGF models.

In this computational study, a comparative assessment of Euler-Euler KTGF and Euler-Lagrange models is performed using small (laboratory) scale fluidized bed (SSFB) and pilot scale circulating fluidized bed (CFB) challenge problems designed for validation. Both problems are particularly suited for modelling using Euler-Euler KTGF and Euler-Lagrange models and for their comparative assessment since the particles considered in both problems are nearly monodisperse (Geldart Group D in SSFB and Group B based cases in CFB). The advantage with monodisperse particle system based comparative assessment of models is that the system remains free of size or density based segregation effects and polydisperse gas-particle drag force related effects. Furthermore, for gas-particle systems, drag force is the most dominant interaction force and it can easily be accounted in an equivalent manner in both models. In SSFB, inventory of particles corresponds to about 93000 particles. Therefore, Euler-Lagrange simulations with Discrete Element Method (DEM) to resolve collisions based on individual particles can be performed in affordable manner. In CFB problem, time-averaged inventory of particles in main riser section is such that the Euler-Lagrange with DEM simulations can only be performed by tracking

trajectories and collisions of group of particles or parcels.

This paper is organized as follows. We begin with a brief description of experimental facilities, flow conditions and experimental measurements. Next, we give an overview of models along with geometry simplification, grid resolutions and boundary conditions considered in simulations. After that, results from SSFB and CFB simulations are presented with the conclusion in the end.

EXPERIMENTAL FACILITY

On NETL website both challenge problems (NETL CFB 2010, NETL SSFB 2013) are well documented including information on test units, geometrical dimensions, instrumentation, and experimental measurements. Here we provide only brief description.

NETL Small Scale Fluidized Bed

A schematic of the rectangular fluidized bed test unit is shown in Figure 1. Physical properties of gas (air) and particles (Geldart Group D) are given in Table 1. Experimental flow conditions are given in Table 2. Gas entering the test unit at the bottom first gets distributed by bottom distributor and then gets redistributed by top distributor above which fluidized bed particles are present. The diameter of each orifice on the top distributor is slightly smaller than the diameter of a particle.

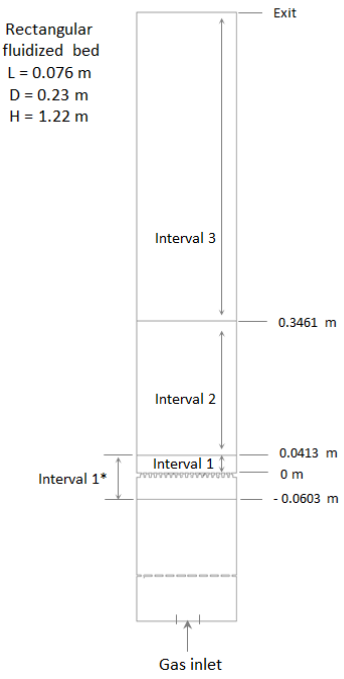

Figure 1: Schematic of small scale fluidized bed test unit.

Table 1: Physical properties of gas and particles

Particle diameter	3.256×10^{-3} m
Particle density	1131 kg/m^3
Gas density	1.2 kg/m^3
Gas viscosity	1.8×10^{-5} kg/m s

Experimental data have been reported in the form of mean and standard deviation of differential pressure (DP) across Interval 1*, Interval 2 and Interval 3; mean and additional statistical quantities of vertical and horizontal velocities of the particles; and granular temperature. The DP across Interval 1* includes DP across distributor and DP across interval 0 m to 0.0413 m which henceforth referred to as Interval 1. Since DP data across Interval 1 are not provided in the experimental data set, we extracted DP data across this interval by subtracting DPs across Intervals 2 and 3 from DP estimated based on total inventory of particles. Such extracted DP data across Interval 1 were used for comparison with simulation predictions.

Table 2: Flow conditions

Case	Solid Weight (Kg)	Gas Superficial Velocity (m/s)
1	1.9	2.19
2	1.9	3.28
3	1.9	4.38

NETL Circulating Fluidized Bed

The NETL circulating fluidized bed test unit is shown in Figure 2. Gas (air) enters the test unit from axial inlet located at the bottom of riser and solids returning from standpipe are recirculated back into the riser from a side inlet. The CFB was operated at five different flow conditions out of which only Case 3 is considered in this study. Case 3[1] corresponds to Group B particles with mean diameter 748 μm and density 863.3 kg/m^3. Superficial velocity of gas and solids circulation rate are 5.71 m/s and 5.54 kg/s, respectively.

MODEL DESCRIPTION

Simulations of both SSFB and CFB were performed using Euler-Euler KTGF model and Euler-Lagrange model with DEM to account for particle or parcel collisions.

Euler-Euler KTGF model

In this modelling approach, gas and particle phases are treated in an Eulerian frame and a set of conservation equations is solved for each phase. The governing equations of this model are well documented (Crowe et

[1] "Case 3" as outlined in https://mfix.netl.doe.gov/challenge/CFB_Challenge_Problem.xls, not Case 3 in Table 2.

al. 1998) and hence will not be repeated here. Gas-particle drag force that couples the motion of phases is the most dominant interaction force for gas-particle system since the Stokes number based on particle is typically large. In this computational study, we explored two drag force formulations.

First one is the widely used Gidaspow drag force formulation (Gidaspow et al., 1992). Second one is the drag force formulation put forth by Tenneti et al. (2011) based on DNS study of flow past fixed random assemblies of monodisperse spheres with finite fluid inertia using immersed boundary method. This drag

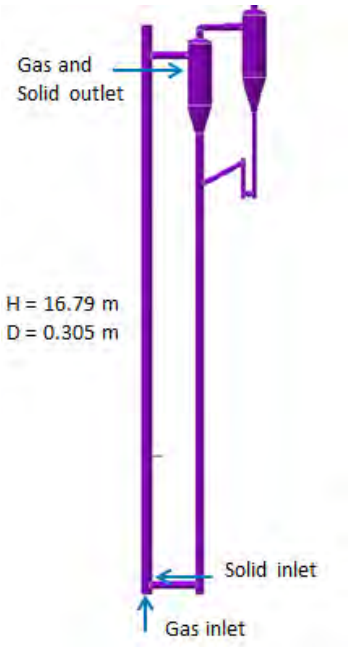

Figure 2: Pilot scale circulating fluidized bed test unit.

force formulation is given as a function of particle volume fraction $\phi\ (0.1 \le \phi \le 0.5)$, and mean flow Reynolds number $\mathrm{Re}_m\ (0.01 \le \mathrm{Re}_m \le 300)$ which is calculated based on particle diameter and magnitude of slip velocity between two phases. In that study, it is shown that the values obtained from Gidaspow drag force formulation begin to differ quite significantly from DNS results in the limits of higher volume fraction $(\phi > 0.2)$ and mean flow Reynolds number. Since both limits are being satisfied in the SSFB problem, for its simulation the use of second drag force formulation is essential. In the CFB problem, average volume fraction of particles remains below 0.2 where Gidaspow drag force formulation does not differ significantly from DNS results over the range of Re_m and thus usage of Gidaspow drag force formulation is adequate.

Euler-Lagrange model

In this modelling approach, the gas phase is treated in Eulerian frame and for the solution of its conservation equations particle volume fraction and velocity information is needed at the centre of each cell in fixed Eulerian grid. This information is provided by averaging over particle field data and then mapping it to Eulerian grid. The particle phase is treated in Lagrangian frame by tracking discrete particles or groups of particles or parcels with their trajectories described by

$$m_p \frac{d\vec{u}_p}{dt} = \vec{F}_d + \vec{F}_p + \vec{F}_{vm} + \vec{F}_g + \vec{F}_{other} + \vec{F}_{contact} \qquad (1)$$

In this equation, terms on right hand side represent drag force, pressure force, virtual mass force, gravitational force, any other forces acting on particle, and particle-particle contact force. The last term is calculated using Discrete Element Method (DEM) based on work of Cundall and Strack (1979). Briefly, the normal contact force on particle 1 which is in contact with particle 2 is calculated using a spring-dashpot model:

$$\vec{F}_1 = \left(K\delta + \gamma\left(\vec{v}_{12} \cdot \vec{e}_{12}\right)\right)\vec{e}_{12} \qquad (2)$$

In tangential direction only sliding contact between particles is considered in this study and tangential contact force is calculated using the equation for Coulomb friction:

$$\vec{F}_{friction} = \mu \vec{F}_{normal} \qquad (3)$$

In simulations involving parcels, the contact force is calculated based on parcel mass and its diameter. The parcel mass is calculated as sum of mass of all particles in a parcel and the parcel diameter is calculated from mass of a parcel and density assumed to be the same as the particle density.

SIMULATIONS

In this computational study, all simulations were carried out using ANSYS Fluent 15.0.

SSFB simulations

First, series of Euler-Euler KTGF model based simulations of Case 1 (considered as a test-bed) were performed to check the effects of drag force formulations and gas-inlet configurations. After these simulations, simulations of Case 2 and Case 3 were performed with one selected gas-inlet configuration and without making any changes to the model. For Case 1 simulations, we considered three different types of gas-inlet configurations. In first type of configuration, only a portion of geometry above top distributor was considered, and without resolving nozzles in geometry, gas mass flow rate corresponding to the superficial velocity given in Table 2 was specified on the whole inlet surface. This configuration is referred to as Uniform Inlet. In the second type of configuration referred to as Distributor Inlet, we kept the geometry as in first configuration but resolved all of the nozzles on the top distributor. In the third type of configuration referred to as Complete Geometry, we considered the whole geometry shown in Figure 1. In all of the configurations, the cell size in the main part of the fluidized bed (above inlet regions) was kept approximately as 3.9 times particle diameter. Total

number of cells in the grids with Uniform Inlet, Distributor Inlet and Complete Geometry were 10000, 48000 and 244000, respectively. For both gas and particle phases, wall boundary condition was set to no-slip.

Euler-Lagrange model simulations require the cell size in the grid to be bigger than the size of particle or parcel. The grid with Uniform Inlet configuration can easily satisfy this requirement but the grids with Distributor Inlet and Complete Geometry configurations cannot. Therefore for these simulations, instead of accurately resolving nozzles, we considered simplified rectangular shaped nozzles as shown in Figure 3 and generated a grid with cell size of about 3.5 times particle diameter. For particle-particle and particle-wall collision calculations, spring constant, coefficient of restitution and coefficient of friction were arbitrarily set to 500 N/m, 0.9 and 0.1, respectively. Particle time step was set to $t_{coll}/5$ where t_{coll} is the collisional time scale that is given by

$$t_{coll} = \left(\frac{m_{12}}{K} \left(\pi^2 + (\ln \eta)^2 \right) \right)^{\frac{1}{2}} \qquad (4)$$

where, reduced mass is calculated from masses of particle 1 and 2: $m_{12} = (m_1 m_2 / (m_1 + m_2))$. All simulations of SSFB were run up to at least 15 sec of flow time calculations and next 10 sec of flow time data were used for time-averaging. Data gathering frequency was set to 1000 Hz.

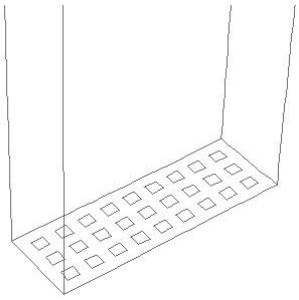

Figure 3: Gas-inlet configuration considered for Euler-Lagrange model based simulations.

CFB simulations

Agrawal et al. (2001) showed that for realistic predictions of gas-particle flows, grid resolution must be of the order of few particle diameters in order to resolve fine scale structures (clusters and streamers) that are shown to further reduce gas-particle drag. For understanding the change in simulation predictions with successive grid refinements and for comparative assessment study, we performed CFB simulations using Euler-Euler KTGF model with three different grid resolutions – coarse, intermediate and refined grids consisting of 65000, 1.67 million and 3 million cells, respectively. The various parameters of these grids are shown in Table 3.

Recently we started CFB simulations using Euler-Lagrange model. Since it is nearly impractical to perform individual particles based simulations, for CFB study, we took parcel based approach. Here we present results from a preliminary simulation run that was performed using 96000 hexahedral cells and 0.47 million parcels with 1826 particles per parcel. Parcel-Parcel collisions were accounted using DEM with spring constant, coefficient of restitution and friction coefficient arbitrarily set to 1000 N/m, 0.7 and 0.25, respectively. Subsequent simulations with lesser number of particles per parcel will need to be performed to understand its effect on simulation predictions. All CFB simulations were run for sufficiently longer time to allow cases to reach statistical steady state before gathering data for time-averaging.

Table 3: The various parameters of grids considered in CFB simulations using Euler-Euler KTGF model.

	Approximate cell lengths			
	Along circumference	Across diameter	Along axis	Grid Size
Coarse	90* d_p	31*d_p	40*d_p	65000
Intermediate	22* d_p	10*d_p	10*d_p	1.67M
Fine	10* d_p	10*d_p	10*d_p	3 M

RESULTS AND DISCUSSIONS

SSFB simulation results

Mean DP values across Interval 2 from experiments and simulations of Case 1 are given in Table 4. Several points emerge from this table after we compare these values. Overall, simulations slightly over predict mean DP values compared to experiments. As expected, the values obtained from simulations using Tenneti et al. drag law are lower compared to those obtained using Gidaspow drag law and closer to experimental data. By comparing the values for three different gas-inlet configurations obtained from Euler-Euler KTGF simulations with Gidaspow or Tenneti et al. drag law, we see that Uniform Inlet always leads to higher solids hold up in that interval compared to other two gas-inlet configurations which give almost same mean DP values. Mean DP values predicted by Euler-Lagrange model with Tenneti et al. drag law for two different gas-inlet configurations do not differ much indicating that assumed size of each rectangular shaped nozzle in Distributor Inlet configuration is too coarse and overall gas-particle flow distribution is same with both inlet configurations. By comparing mean DP values from Euler-Lagrange and Euler-Euler KTGF models, it can be said that predictions from both models are comparable.

Figure 4 shows snapshots of volume fraction of particle- phase obtained from simulations using Euler-Euler KTGF model with Tenneti et al. drag law for three different inlet configurations. In case of Uniform Inlet, we see constant presence of thin uniform layer consisting of lower volume fraction of particle-phase

next to inlet surface. This forces more particles into Interval 2 and hence leads to higher hold up predictions in that interval. With other two inlet configurations, gas streams emerging from nozzles merge together and periodically generate bubbles that rise upward and eventually burst into free board region. We see that the particles flow upward in centre region and downward adjacent to walls. Since there is no significant difference between Distributor Inlet and Complete Geometry results, we performed simulations of Case 2 and Case 3 using Distributor Inlet configuration and Tenneti et al. drag law with Euler-Euler KTGF as well as Euler-Lagrange model. In simulations of Case 2 and 3, fluidization behaviour looked significantly different from Case 1. At higher superficial velocities both models predict vigorous fluidization as opposed to periodic generation of bubbles seen in Case 1.

Table 4: Mean DP across Interval 2 from experiments and simulations of Case 1.

Case 1	Mean DP across Interval 2 (kPa)
Experiments	0.686
Euler-Euler KTGF model with Gidaspow drag law	
Uniform Inlet	0.916
Distributor Inlet	0.862
Complete Geometry	0.857
Euler-Euler KTGF model with drag law proposed by Tenneti et al.	
Uniform Inlet	0.844
Distributor Inlet	0.783
Complete Geometry	0.794
Euler-Lagrange model with drag law proposed by Tenneti et al.	
Uniform Inlet	0.856
Distributor Inlet - Square nozzles	0.873

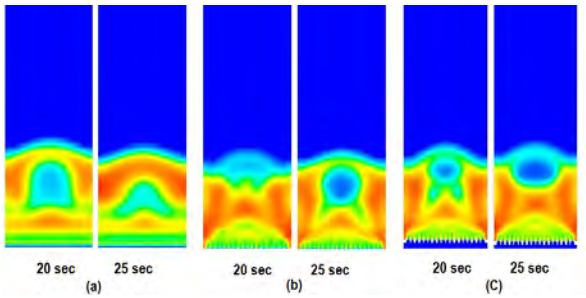

Figure 4: Snapshots of particle-phase volume fraction at 20 and 25 sec of flow time from simulations using Euler-Euler KTGF model with Tenneti et al. drag law. (a) Uniform Inlet. (b) Distributor Inlet. (c) Complete Geometry (bottom portion not shown).

Figure 5 shows comparison of mean DP predictions obtained from Euler-Euler KTGF model based simulations of three cases (listed in Table 2) with the experimental data. In this figure, filled symbols represent experimental data and open symbols with lines represent simulations. Circles are for mean DP across Interval 1, squares are for Interval 2 and triangles are for Interval 3. In experiments, with increase in superficial velocity, mean DP increases across Intervals 1 and 3, and decreases across Interval 2. Euler-Euler KTGF model qualitatively captures the trends for the Intervals 1 and 3 but does not predict significant decrease in mean DP across Interval 2 as seen with experimental data.

Figure 6 shows predictions from Euler-Lagrange model simulations. These simulations do predict decrease in mean DP across Interval 2 with the increase in superficial velocity. From last two figures, we see that both Euler-Euler KTGF and Euler-Lagrange models predict comparable mean DP values for all three intervals but when compared with experimental data, quantitative

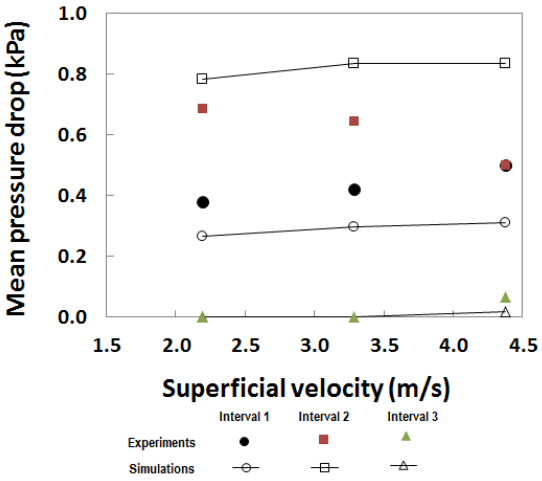

Figure 5: Effect of superficial velocity on mean DP across three intervals. Simulation predictions are from Euler-Euler KTGF model.

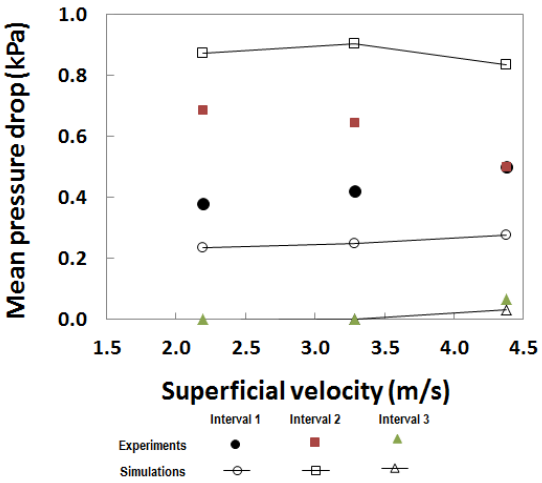

Figure 6: Effect of superficial velocity on mean DP across three intervals. Simulation predictions are from Euler-Lagrange model.

differences are clearly visible. We have not yet explored the effect of wall boundary conditions as well as Euler-Euler KTGF model parameters such as coefficient of restitution, which might play some role in the model

predictions. Similar study with Euler-Lagrange approach is also needed.

Figure 7 shows comparison of standard deviation of DP across Interval 2 obtained from Euler-Euler KTGF and Euler-Lagrange models with experimental data. Predictions from both models are in good agreement with experimental data at smallest and largest superficial velocities but not at intermediate superficial velocity.

We now compare time-averaged particle-phase vertical velocity predictions obtained from Euler-Euler KTGF and Euler-Lagrange models with the experimental data. In experiments, particle-phase velocity measurements were performed using high speed PIV that traced particles appearing in cells (0.0457 m X 0.0457 m X 0.003 m)

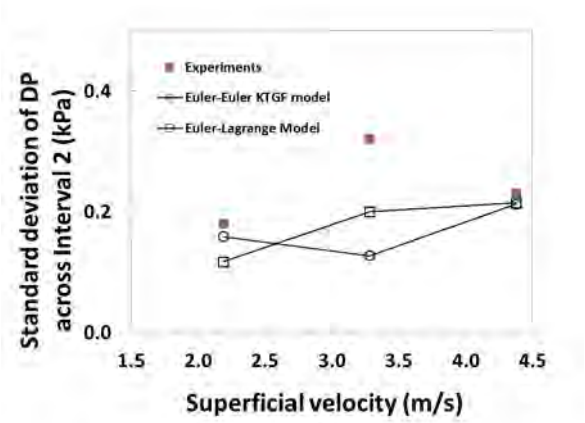

Figure 7: Effect of superficial velocity on standard deviation of DP across Interval 2.

located adjacent to the wall and at the mid-point elevation of 0.0762 m measured from top distributor. Since these measurements were performed within a particle diameter distance from the wall, the measurements were expected to be strongly influenced by particle-wall interactions.

Figure 8 shows comparison of time-averaged particle-phase vertical velocity profiles obtained from Euler-Euler KTGF model based simulations with the experimental data. Since these profiles are from near wall regions and in simulations we used no-slip boundary condition for both phases, as expected, we see under prediction of velocities at all lateral locations. Since in Euler-Lagrange simulations particles were allowed to slip with specified particle-wall collision parameters, we see visible improvements in velocity predictions in Figure 9. Slight asymmetry in velocity profiles indicates that the considered time interval for simulation data gathering was not long enough.

CFB simulation results

To understand the change in simulation predictions with successive grid refinements and for comparative assessment of the models, we performed a set of simulations using Euler-Euler KTGF model with coarse, intermediate and refined grids consisting of 65000, 1.67 million and 3 million cells, respectively. Figure 10 shows time-averaged gas-phase axial pressure gradient profiles obtained from these simulations. In this figure, experimental data is also shown for comparison. With successive global grid refinements we see improvements in pressure gradient predictions, however even with refined grid where cell size is about ten times particle diameter, the model under predicts the hold up.

Predictions from Euler-Lagrange model are also given in Figure 10. The Euler-Lagrange simulations were performed on a coarse grid consisting of 96000 cells and

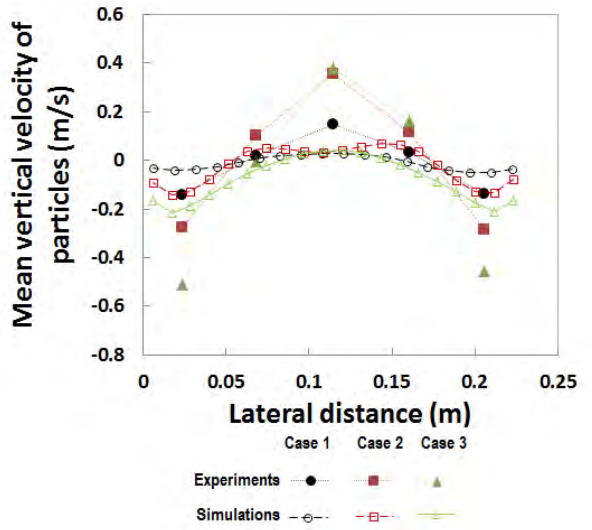

Figure 8: Comparison of time-averaged particle-phase vertical velocity profiles obtained from Euler-Euler KTGF simulations with experimental data. Profiles are from regions adjacent to the wall.

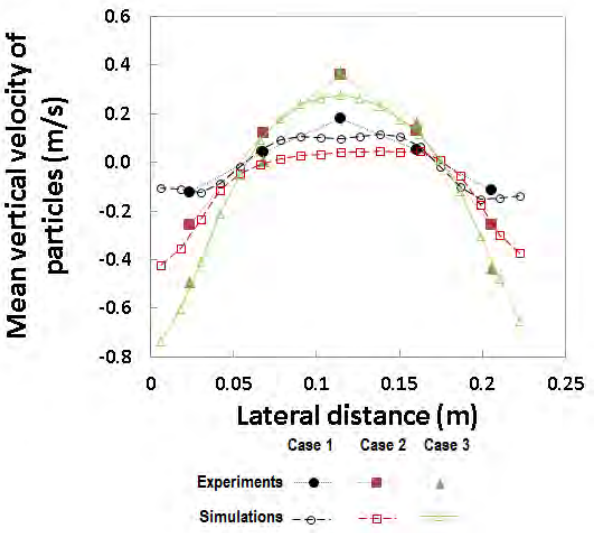

Figure 9: Comparison of time-averaged particle-phase vertical velocity profiles obtained from Euler-Lagrange simulations with experimental data. Profiles are from regions adjacent to the wall.

0.47 million parcels. We see that the predictions from Euler-Lagrange model are comparable to those obtained

from Euler-Euler KTGF model using coarse grid. Comparison of time-averaged particle-phase axial velocity profiles obtained at 8.88 m elevation is shown in Figure 11. These preliminary results indicate that further studies with Euler-Lagrange model are also needed to understand the effects of grid and boundary layer resolution along with the number of parcels on model predictions.

SUMMARY

Euler-Euler KTGF and Euler-Lagrange models gave similar results for gas-particle flows in small scale fluidized bed (SSFB) and pilot scale circulating fluidized bed (CFB). In SSFB study, the results were found to be in qualitative agreement with the experimental data. Resolving nozzles on gas distributor and using DNS based drag law proposed by Tenneti et al. (2011) led to further improvement in results. In CFB study, both models gave similar results with coarse grid resolution. Euler-Euler KTGF model predictions improved with successive global grid refinements; however additional elaborate study is needed to understand the effects of various parameters including resolution of boundary layer cells. Similar CFB study with Euler-Lagrange model is needed to understand the effects of grid and boundary layer resolution, number of parcels, and parameters used in DEM calculations.

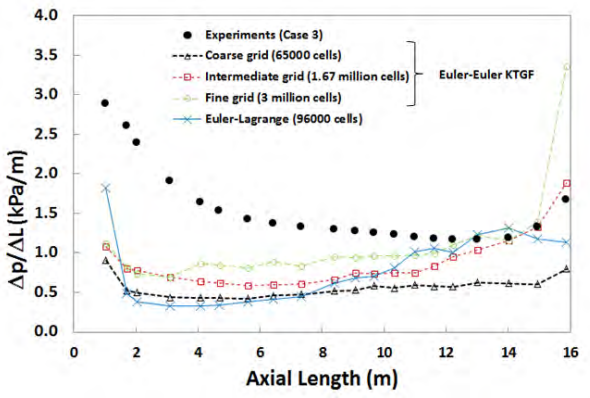

Figure 10: Predictions of time-averaged gas-phase axial pressure gradient from Euler-Euler KTGF and Euler-Lagrange simulations. Experimental data is also shown for comparison.

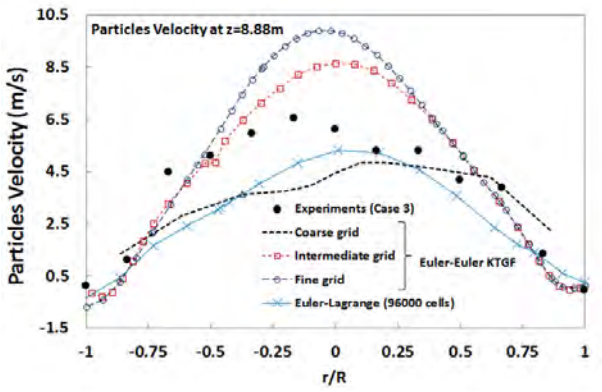

Figure 11: Predictions of time-averaged particle-phase axial velocity from Euler-Euler KTGF and Euler-Lagrange simulations. Experimental data is also shown for comparison.

REFERENCES

AGRAWAL, K., LOEZOS, P. N., SYAMLAL, M. and SUNDARESAN, S., (2001), "The role of mesoscale structures in rapid gas-solid flows", *J. Fluid Mech.*, **445,** 151-185.

CROWE, C., SOMMERFELD, M. and TSUJI, Y., (1998), "Multiphase Flows with Droplets and Particles", CRC Press.

CUNDALL, P.A. and STRACK, O.D.L., (1979), "A discrete numerical model for granular assemblies. *Geo-technique*, **29,** 47-65.

GIDASPOW, D., BEZBURUAH, R. and DING, J., (1992), "Hydrodynamics of circulating fluidized beds, kinetic theory approach", *In Fluidization VII, Proceedings of the 7th Engineering Foundation Conference on Fluidization*, 75–82.

IGCI, Y. and SUNDARESAN, S.,(2011), "Constitutive models for filtered two-fluid models of fluidized gas-particle flows", *Ind Eng Chem Res.*, **50,** 13190-13201.

LI, J. and KWAUK, M., (1994), "Particle-Fluid two-phase flow: Energy-Minimization Multiscale Method", Beijing, P. R. China, Metallurgical Industry Press.

MILIOLI, C., MILIOLI, F., HOLLOWAY, W., AGRAWAL, K. and SUNDARESAN, S., (2013), "Filtered two-fluid models of fluidized gas-particle flows: New constitutive relations", *AIChE J.*, **59,** 3265-3275.

NETL CFB 2010 challenge problem https://mfix.netl.doe.gov/challenge/index_2010.php

NETL SSFB 2013 challenge problem https://mfix.netl.doe.gov/challenge/index.php

PARMENTIER, J-F., SIMONIN, O. and DELSARTK, O., (2012), "A functional subgrid drift velocity model for filtered drag prediction in dense fluidized bed", *AIChE J.*, **58**, 1084-1098.

TENNETI, S., GARG, R. and SUBRAMANIAM, S., (2011), "Drag law for monodisperse gas-solid systems using particle-resolved direct numerical simulation of flow past fixed assemblies of spheres", *Int. J. Multiphase Flow*, **37,** 1072-1092.

WEN, C.-Y. and YU, Y. H., (1966), "Mechanics of fluidization", *Chem. Eng. Prog. Symp. Series.*, **62**, 100–111.